HAL
open science

Cloud Detection from the Spaceborne POLDER Instrument and Validation against Surface Synoptic Observations

Francois-Marie Breon, Stéphane Colzy

To cite this version:

Francois-Marie Breon, Stéphane Colzy. Cloud Detection from the Spaceborne POLDER Instrument and Validation against Surface Synoptic Observations. Journal of Applied Meteorology, 1999, 38 (6), pp.777-785. 10.1175/1520-0450(1999)0382.0.CO;2 . hal-03119834

HAL Id: hal-03119834

https://hal.science/hal-03119834

Submitted on 25 Jan 2021

HAL is a multi-disciplinary open access archive for the deposit and dissemination of scientific research documents, whether they are published or not. The documents may come from teaching and research institutions in France or abroad, or from public or private research centers.

L'archive ouverte pluridisciplinaire **HAL**, est destinée au dépôt et à la diffusion de documents scientifiques de niveau recherche, publiés ou non, émanant des établissements d'enseignement et de recherche français ou étrangers, des laboratoires publics ou privés.

Cloud Detection from the Spaceborne POLDER Instrument and Validation against Surface Synoptic Observations

FRANÇOIS-MARIE BRÉON AND STÉPHANE COLZY

Laboratoire des Sciences du Climat et de l'Environnement, Direction des Sciences de la Matière, Commissariat à l'Energie Atomique, Gif-sur-Yvette, France

(Manuscript received 26 January 1998, in final form 29 September 1998)

ABSTRACT

This paper describes the cloud screening algorithms that have been developed for the processing of Polarization and Directionality of the Earth Reflectances (POLDER) measurements over land surfaces. Four tests are applied to the measurements. The first one is a threshold on the 0.44-μm reflectance after atmospheric correction. The second one is similar but with a smaller threshold and is applied only over targets with significant spectral variation. The third one compares the surface pressure to an estimate derived from two POLDER channels centered on an oxygen absorption band. The fourth one makes use of POLDER polarization capabilities and seeks the presence of a rainbow generated by water clouds.

The performance of the method is evaluated using a large dataset of nearly coincident POLDER measurements and surface observations of cloud cover. The validation dataset is fully independent of the spaceborne measurements and allows the sampling of a wide range of situations. The results demonstrate the capability of the algorithm to distinguish clear and cloudy pixels, although a large fraction of pixels with a small cloud cover are incorrectly declared clear. This may be due in part to the different field of view of the spaceborne and surface observations. For a given cloud cover, the detection is less efficient for high clouds than for low- or medium-altitude clouds, which may result from their lower-optical thickness.

1. Introduction

The POLDER instrument [Polarization and Directionality of the Earth Reflectances (Deschamps et al. 1994)] is an optical instrument that was launched in August 1996 on the Advanced Earth Observing Satellite (ADEOS) platform with the objective of monitoring earth surfaces and the atmosphere.

POLDER measurements are processed by three parallel sets of algorithms with different scientific objectives.

- ocean color and aerosols over the oceans (from clear measurements over the ocean);
- land surface reflectances and directional signatures, atmospheric water vapor, and aerosols over land (from clear measurements over land surfaces) (Leroy et al. 1997);
- cloud optical and physical parameters and earth radiation budget (Buriez et al. 1997).

Each set of processing algorithms includes cloud detection, the result of which controls further processing. For the two first sets of algorithms, measurements recognized as cloud contaminated are not used for further processing. Over the ocean, cloud detection is relatively easy since the background reflectance is low and well predictable, especially in the near infrared. Over land surfaces, the variability of surface reflectance makes cloud detection more difficult, especially in the case of semitransparent clouds, or broken cloudiness.

In this paper, we present the method for cloud detection that is used to process POLDER measurements over land surfaces, with the final objective of retrieving the surface reflectance and directional signature. Numerous works have been published on cloud detection applied to spaceborne imagery, in particular for the (AVHRR) (see, for instance, Saunders and Kriebel 1988; Derrien et al. 1993; Simpson and Gobat 1996). These methods cannot be applied directly to POLDER measurements because of the lack of thermal infrared channels. On the other hand, POLDER has more channels in the solar spectrum, they are narrower, and the instrument measures the polarization state of the reflected light. These capabilities allow the use of novel cloud detection methods.

The validation of cloud detection algorithms is not an easy task because there is no independent measurement with the same spatial resolution. In most cases, the performances of cloud detection algorithms have been evaluated against visual analysis of the original

Corresponding author address: Dr. Francois-Marie Bréon, CEA/DSM/LSCE, Gif sur Yvette F-91191, France.
E-mail: fmbreon@cea.fr

© 1999 American Meteorological Society

2+54/.240,+4.-7&3621 3+-.- !"#"! "$!#(')%

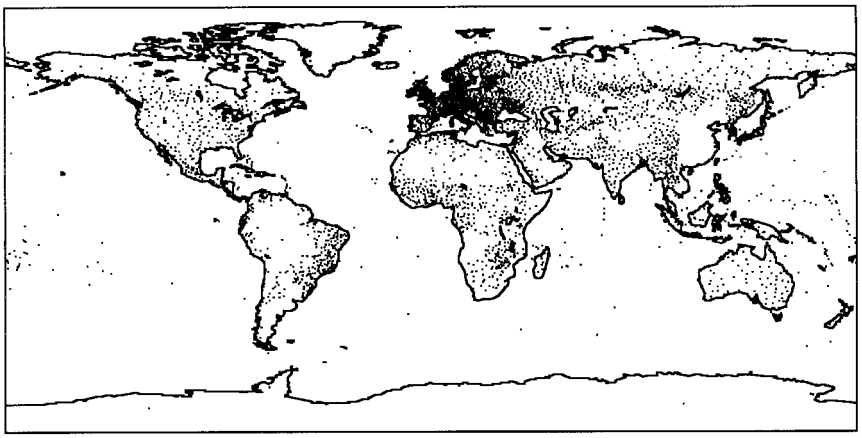

FIG. 1. Geographical distribution of meteorological stations that provide cloud-cover reports to the worldwide synoptic network.

satellite images (see for instance Saunders and Kriebel 1988). The human eye is able to recognize on a satellite image cloud structure much better than any automatic algorithm does, which justifies this validation approach. However, the dataset used for the validation is not independent, and the human cloud recognition may miss the difficult cases (thin clouds, broken cloudiness). Besides, the comparison requires a large amount of tedious work, which is unsuited for a quantitative validation on a large dataset. For these reasons, we decided to base our validation procedure on the comparison with near-coincident surface observations of cloud cover. We believe that cloud recognition from the surface is much easier than from space, because contrary to land surfaces, the clear sky provides a uniform and relatively dark background. This approach has been used on a limited scale in Derrien et al. (1993) and Visa and Iivarinen (1997).

Section 2 presents the surface observations used for threshold adjustment and validation. Section 3 is a brief presentation of POLDER measurement characteristics. Section 4 describes the cloud detection algorithm. The validation results are presented in section 5 and discussed in section 6. Section 7 summarizes the results and concludes the article.

2. Surface synoptic observations

The worldwide meteorological network includes a large number of stations that report information on the current weather including cloud cover and cloud type. Figure 1 shows the geographical distribution of these stations. The largest density is found in Europe but stations are found in most geographical areas, even sparsely populated.

The cloud-cover observation is expressed in octants. The nine possible values (from 0 to 8 octant) have been converted to percentage on the Meteo-France database (0%, 10%, 25%, 40%, 50%, 60%, 75%, 90%, 100%). Note that 1 octant (10%) indicates that at least one cloud can be observed, even covering a very small fraction of the sky. Similarly, 7 octants (90%) indicates that the cloud cover is not overcast. In the following, we have corrected the 40% and 60% values to 37.5% and 62.5%, which is statistically closer to the original observation. No change was applied to the 10% and 90% values since they are representative of the extremes (down to 1% and up to 99%).

Figure 2 shows a statistic of cloud-cover distribution as a function of latitude and season. Because the stations are not evenly distributed along the longitudes (in particular, there are very few stations over the oceans), the statistical values may not be fully representative of the globe. However, some main features of the earth's climate are depicted in Fig. 2, such as the relative maximum of clear occurrence in the subtropics, corresponding to the subsidence zone of Hadley cells, and the maximum of cloud cover in the equatorial regions. Note that in the polar regions, a relatively large fraction of clear occurrence is found. This is observed mostly during the polar night, which raises some doubts on the data validity.

In the context of optical remote sensing of the surfaces, the main result is the very small fraction of clear occurrence. If all cloud-contaminated observations were to be discarded, less than 10% of the satellite measurements could be used. This results should be somewhat adjusted with regard to the different field of view of the satellite instrument and the surface observer. This point is discussed in section 6.

3. POLDER measurements

POLDER is an optical instrument launched on the ADEOS platform in August 1996. It provided continuous measurements of the earth spectral, directional, and polarization signature before the ADEOS platform unexpectedly failed at the end of June 1997. Another POL-

2+54/.240,+4.-7&3623+-.- !"#"! "$!#(')%

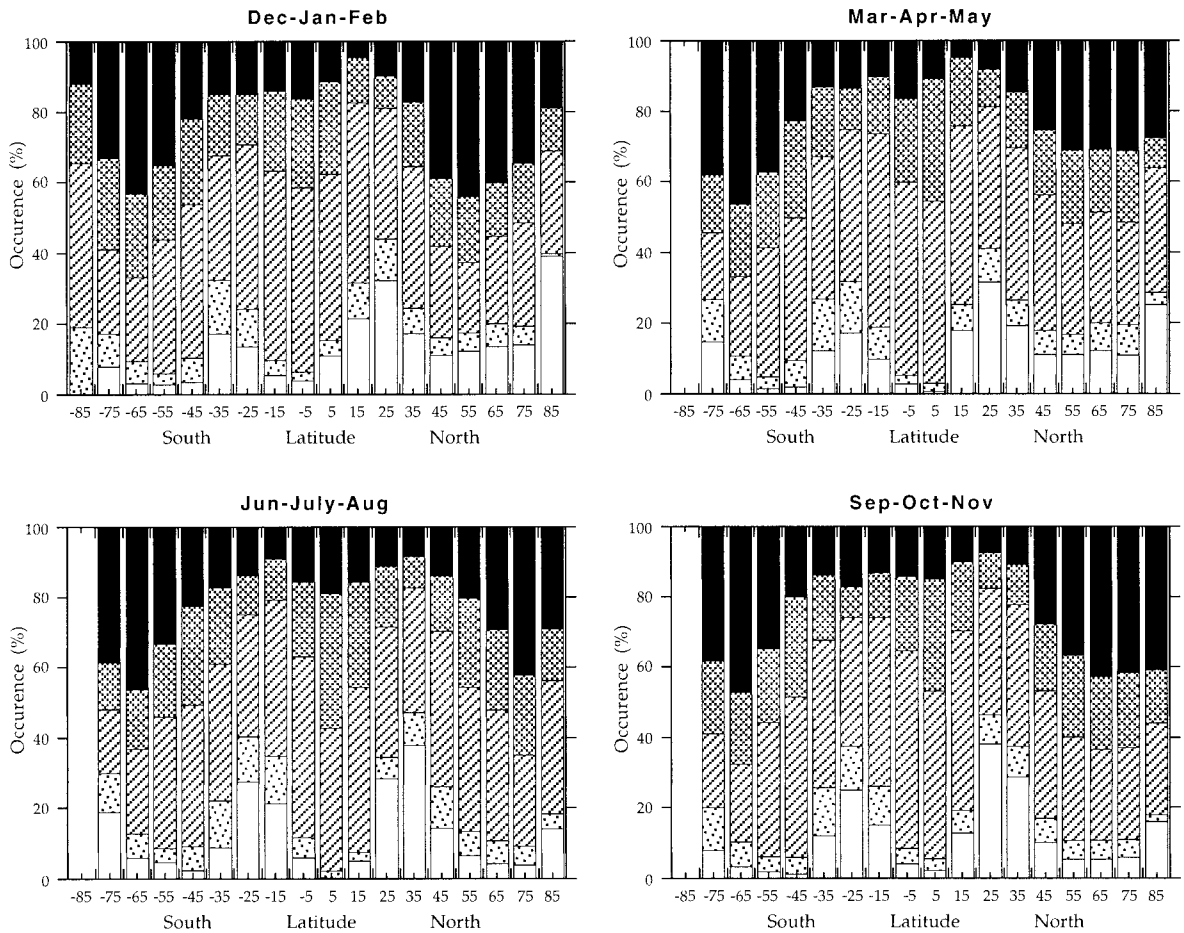

FIG. 2. Statistical distribution of cloud-cover occurrence as reported by the meteorological stations. The stations have been classified into 18 10° latitude bands. The four figures correspond to four 3-month periods: Dec–Feb (Fig. 3a), Mar–May (Fig. 3b), Jun–Aug (Fig. 3c), and Sep–Nov (Fig. 3d). The five classes (bottom to top) correspond to clear, 1 octa, 2–6 octas, 7 octas, and overcast.

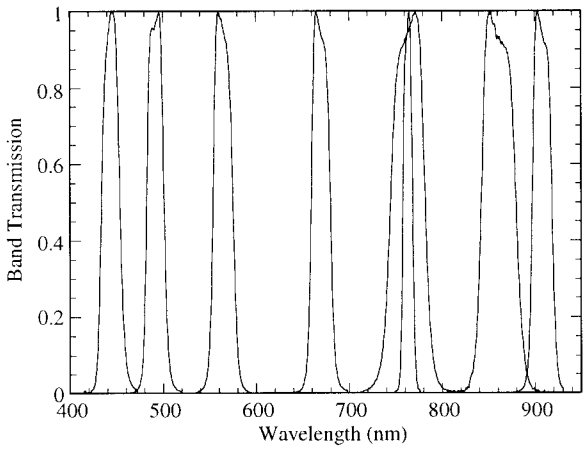

FIG. 3. Spectral response of the eight POLDER channels. Three of these channels provide linear polarization characteristics (0.44, 0.67, and 0.86 μm).

DER instrument, similar to the first one, is scheduled to be launched on the ADEOS-2 platform in 2000.

The POLDER instrument concept (a CCD bidimensional matrix and a wide field of view lens) permit the acquisition of up to 14 successive measurements of a given target as the satellite goes along its orbit. This allows an evaluation of the target directional signature. Another original feature of POLDER is its capacity to measure the polarization state of the reflectance (linear polarization ratio and direction). The main objective of polarization measurements is the remote sensing of aerosols over land surfaces. However, this piece of information can also be used for an estimate of the cloud phase, the cloud top pressure (Buriez et al. 1997), or the cloud droplet radius (Bréon and Goloub 1998).

The POLDER instrument acquires measurements in eight spectral bands from 440 nm to 910 nm (Fig. 3). Polarization measurements are performed in three of these bands (440, 670, and 865 nm). The spectral resolution is 6.2×6.2 km^2 after registration of the multidirectional measurements on an earth-fixed grid. The

2+54/.240,+4.-7&3623+-.- !"#"! "$!#(')%

absolute registration error is better than 1 pixel. The multispectral and multidirectional collocation error is better than 0.1 pixel.

Over land, POLDER measurements are processed with the objectives of 1) mapping the aerosol optical thickness and type; 2) assessing the atmospheric water vapor content; and 3) measuring the surface hemispheric reflectance and directional signature (Leroy et al. 1997). The data processing algorithms require the preliminary rejection of cloud-contaminated measurements. This is achieved from an evaluation of the spectral, directional, and polarization signature of the measurements.

4. Cloud detection methods

In the following, we make use of collocated POLDER measurements and surface observations of cloud cover. The difference in time between the two is less than one hour. The POLDER pixel (6.2×6.2 km^2) includes the station from which the visual observation of cloud cover was made.

a. Blue channel reflectance

The shorter wavelength POLDER channel is centered at 0.44 μm (blue band) and is 0.02 μm wide. At this wavelength, most surfaces have a rather low reflectance (Bowker et al. 1985). In fact, the reflectance of both vegetation and bare soils tend to increase with the wavelength within the visible and near infrared spectrum (with a local maximum of vegetation reflectance in the green). On the other hand, the cloud reflectance show very limited variation across this spectrum. Therefore, the contrast between clear and cloudy scenes is the largest in the band 0.44 μm. Note, however, that snow cover is an exception to this rule. The snow reflectance is rather high with limited variation in the visible and a decrease in the near infrared.

The principle of the test is to compare the reflectance measured at 0.44 μm to a threshold. However, the atmospheric reflectance generated by molecular scattering is rather high at this wavelength (often larger than the surface reflectance) and varies with the viewing geometry. It is predictable with a high level of accuracy if the surface pressure is known. The surface pressure is mostly a function of altitude and is known with an accuracy better than 2% in most cases through

$$P_{\text{surf}} = 1013 \exp\left(-\frac{\text{Alt}}{H}\right), \tag{1}$$

where Alt is the pixel mean altitude, and H is the scale height of the molecular atmosphere.

The pixel is recognized cloudy if

$$R_{0.44}^{\text{mes}} - R_{0.44}^{\text{mol}} > \Delta R_{0.44}, \tag{2}$$

where $R_{0.44}^{\text{mes}}$ is the reflectance measurement, $R_{0.44}^{\text{mol}}$ is the molecular reflectance modeled as a function of the surface pressure and the viewing geometry, and $\Delta R_{0.44}$ is a threshold currently set to 0.15. The test is applied to the POLDER measurement that was acquired with the smallest view zenith angle. Figure 4 shows the difference $R_{0.44}^{\text{mes}} - R_{0.44}^{\text{mol}}$ as a function of cloud cover derived from a large set (24 000 pairs) of matched POLDER and synoptic observations. The horizontal line indicates the 0.15 threshold. All pixels corresponding to the dots above the line are declared cloudy by the test. As expected, the reflectance difference increases with the cloud cover. Note that the reflectance difference is not always greater than the threshold even for large cloud covers. This is interpreted as the occurrence of thin clouds such as cirrus. On the other hand, there are a few pixels that are declared as clear by the surface observer with a nevertheless high reflectance. An analysis of these points showed that most of them were in snow-covered areas. The few others may be explained either by the time difference between the two observations or by an inaccurate report.

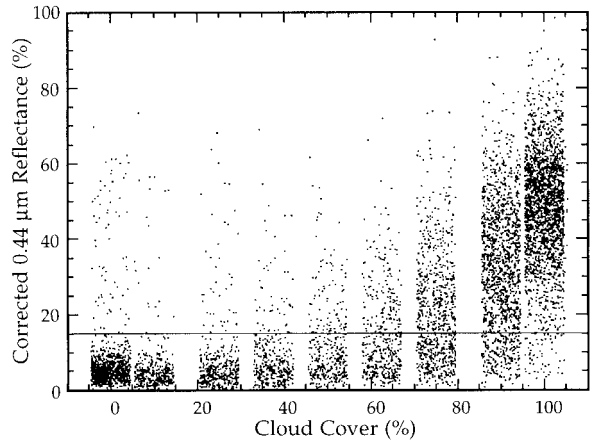

FIG. 4. The $R_{0.44}^{\text{mes}} - R_{0.44}^{\text{mol}}$ difference derived from POLDER measurements as a function of reported cloud cover for matching surface and spaceborne measurements. A random number between −5 and 5 has been added to the cloud-cover notations so that the density of points can be analyzed. The horizontal line shows the threshold that has been chosen for POLDER algorithms.

We tried to lower the threshold, with the objective of being more sensitive to small cloud optical thicknesses. However, some desert areas have a blue reflectance on the order of 0.12, which leads to a lower limit value for the threshold. On the other hand, these areas show a limited increase of the reflectance with the wavelength. Following this observation, an additional test was defined. The pixel is recognized cloudy if

$$R_{0.44}^{\text{mes}} - R_{0.44}^{\text{mol}} > \Delta R_{0.44}^{*}$$

and

$$(R_{0.86}^{\text{mes}} - R_{0.86}^{\text{mol}}) - (R_{0.67}^{\text{mes}} - R_{0.67}^{\text{mol}}) > \Delta\text{dif}, \tag{3}$$

where the 0.67 and 0.86 subscripts refer to the POLDER bands at the corresponding wavelengths. The second inequality excludes desert areas (Δdif is set to 0.1). The

2+54/.240,+4.-7&3623+-.- !"#"! "$!#(')%

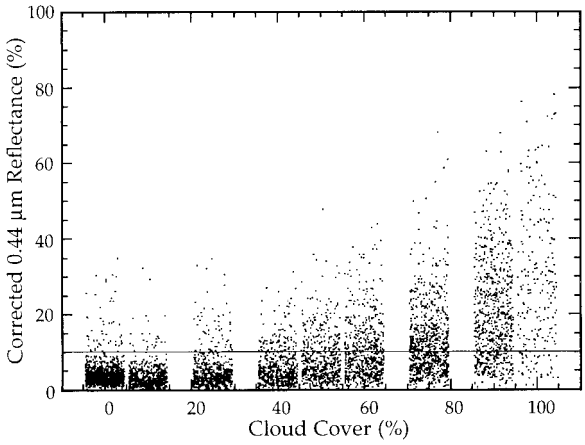

FIG. 5. Same as Fig. 4 but only the pixels with a significant reflectance spectral variation [see Eq. (3)] have been selected.

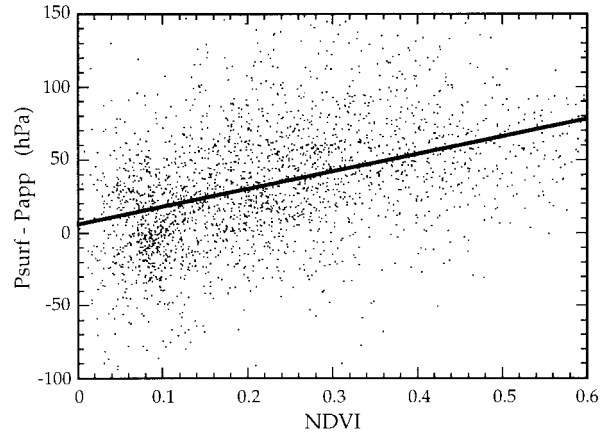

FIG. 6. Scatterplot of $P_{surf} - MP_{app}$ as a function of the NDVI derived from POLDER measurements when the coincident surface observation reported clear sky.

quantity $\Delta R^*_{0.44}$ was set to 0.1, which seems to be a suitable value for vegetated areas as shown in Fig. 5.

b. Main reflector apparent pressure

Two of the POLDER channels are centered on the oxygen A absorption band at 0.76 μm. One is 0.01 μm wide, whereas the other is 0.04 μm wide. It is initially assumed that surface and cloud reflectances averaged over both channels are nearly equal. Therefore, the ratio of the two measurements is a function of the atmospheric transmission, which is essentially controlled by oxygen absorption (Bréon and Bouffiès 1996). Since oxygen is well mixed in the atmosphere, the transmission is a function of the observation geometry and the pressure of the reflector. An analytical function has been derived, which yields the pressure P_{app} to the viewing geometry and the measurement ratio

$$P_{app} = f\left[X, \frac{1}{\cos(\theta_s)} + \frac{1}{\cos(\theta_v)}\right] \tag{4}$$

with

$$X = \frac{R_N^{mes} - R_N^{mol}}{R_W^{mes} - R_W^{mol}}, \tag{5}$$

where N and W refer to the narrow and the wide band, respectively. In order to reduce the random uncertainty, the apparent pressure is averaged over the available directions, which yield MP_{app}. The pixel is then declared cloudy if

$$P_{surf} - MP_{app} > \Delta P, \tag{6}$$

where ΔP is a threshold to be adjusted based on the measurements. An analysis of the $P_{surf} - MP_{app}$ difference for clear cases shows a significant correlation with the vegetation cover quantified by the Normalized Difference Vegetation Index (NDVI) (Fig. 6). Around 0.765 μm, the spectral variation of vegetation reflectance shows a strong negative second derivative (the reflectance increases rapidly with the wavelength around 0.7 μm and levels off around 0.8 μm). Therefore, the surface reflectance averaged over the narrow channel is significantly larger than its equivalent over the wide channel. This yields a larger value of X than that obtained over a surface with a reflectance spectral variation either constant or linear. The apparent pressure is then smaller (Bréon and Bouffiès 1996). As a consequence, the threshold must depend on the NDVI. An empirical analysis of the clear cases yields

$$\Delta P = 60 + 120\text{NDVI}. \tag{7}$$

Figure 7 shows $P_{surf} - MP_{app} - \Delta P$ as a function of cloud cover for matching POLDER and surface observations. There is a general increase with the cloud cover, although many observations yield a negative difference even for large cloud covers. This is expected for low-altitude cloudiness, which can hardly be detected by this test.

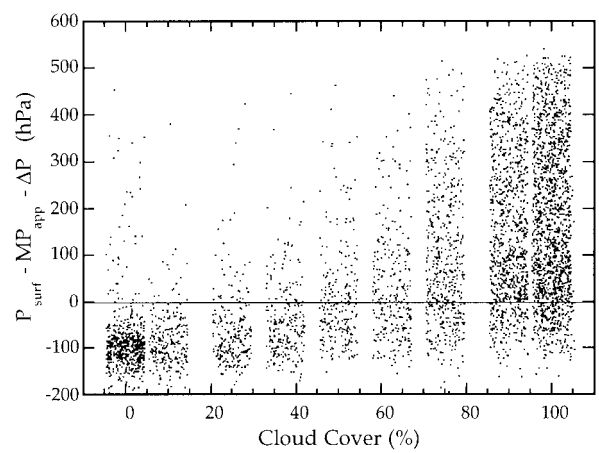

FIG. 7. Same as Fig. 4 but for the parameter $P_{surf} - MP_{app} - \Delta P$, which is used for the ''apparent pressure'' test.

2+54/.240,+4.-7&3623+-.- !"#"! "$!#(')%

c. Polarization signature

The scattering of light by cloud water droplets shows a strong maximum about 142° from the incoming direction (Goloub et al. 1994). In the geometric optic approximation, this is generated by refraction–reflection–refraction within a single droplet. Moreover, this maximum is highly polarized, which makes it easily detectable by a multidirectional, polarization-able instrument such as POLDER. Although more than 11 successive observations are available for most pixels, the needed scattering angle of approximately 142° is acquired for about 60% of the observed pixels. Note that these pixels change from one day to another because of the varying position of the satellite track.

If the required geometry is sampled, the cloud detection method consists in the comparison of the polarization signature in and away from the selected direction. The 0.86-μm channel is used because it is the least affected by atmospheric (molecular and aerosols) scattering. Because the polarized reflectance (R_P) is mostly generated by single scattering or reflection, it has been shown that $[\cos(\theta_s) + \cos(\theta_v)]R_P$ is a function of the scattering angle and almost independent of θ_s or θ_v (Bréon and Goloub 1998). The cloud test compares, therefore, the corrected measurement $[\cos(\theta_s) + \cos(\theta_v)]R_P$ in and away from the 142° scattering angle direction. If the difference is found larger than a threshold (currently set to 5×10^{-3}), the pixel is recognized cloudy. We note that, because this test is only sensitive to liquid water droplets, it cannot detect ice clouds such as cirrus. On the other hand, note that the amount of reflected light generated by single scattering saturates very rapidly with an increase of optical thickness (for an optical thickness on the order of 1). Since the useful signal for the polarization test is mostly generated by single scattering, the test may be equally sensitive to low and large optical thickness clouds, which is not the case for the other tests described above.

Figure 8 shows the variation of the corrected polarized reflectance as measured close to and away from the 142° scattering angle direction. This figure demonstrates that a large difference is an unambiguous indication of a cloud presence. On the other hand, many pixels with a large cloud cover display no polarization signature. These are interpreted as ice clouds.

d. Snow cover recognition

The blue channel reflectance test will fail in the case of snow-covered surfaces. The snow has a large reflectance with a spectral signature similar to that of the clouds in the POLDER spectral range. Therefore, a clear pixel with a snow-covered surface may be recognized as cloudy with the above described method. We have not been able to imagine any criteria that could discriminate intermediate cases (broken and/or thin cloud covers and partial snow covers). On the other hand, the various tests' coherence should discriminate thick clouds and snow-covered surfaces, that is, situations with a large reflectance.

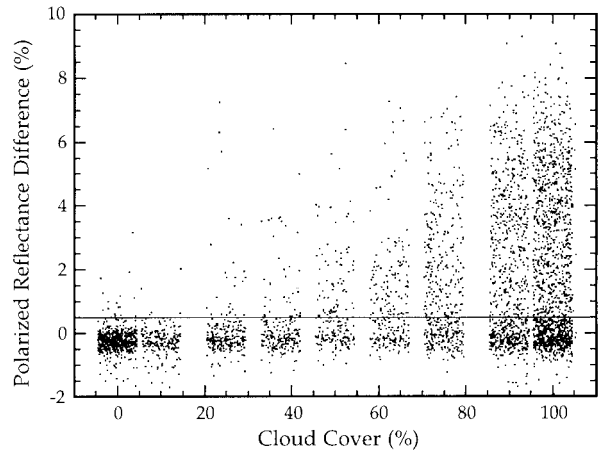

FIG. 8. Same as Fig. 4 but for the difference of the corrected polarized reflectance ($[\cos(\theta_s) + \cos(\theta_v)]R_P$), which have been measured close and away from the rainbow direction. This difference is used for the polarization-based test.

A pixel, initially recognized as cloudy, will be declared snow covered if

- all four tests have been evaluated (i.e., the viewing geometry is suitable for the polarization test),
- only the blue channel tests have recognized the pixel as cloudy (either one or both),
- both $R_{0.67}$ and $R_{0.86}$ are greater than 0.3,
- $R_{0.86} - R_{0.67} < 0.1$.

If the viewing geometry is not suitable for the polarization test, there is no method to discriminate low clouds and snow-covered surfaces, in which case, the pixel will be declared cloudy and not used for further processing.

e. Test combination

All four cloud detection tests are applied to the POLDER measurements. Any one positive test sets the pixel as ''cloudy.'' The ''snow-cover recognition'' algorithm is then applied, which can label as clear (snow-covered surface) a pixel initially recognized as cloudy.

5. Cloud detection validation

The performance of the cloud detection algorithms is hereafter presented as the percentage of pixels that have been recognized cloudy as a function of the synoptic cloud cover. If the algorithm performance were perfect, and if there were no noise sources (resulting from the spatial and temporal differences or inaccurate cloud-cover report), the percentage would be 0 for clear cases and 100 for any positive cloud cover. In practice, the percentage increases with the cloud cover, and we seek a compromise between a small percentage for clear cas-

2+54/.240,+4.-7&3623+-.- !"#"! "$!#(')%

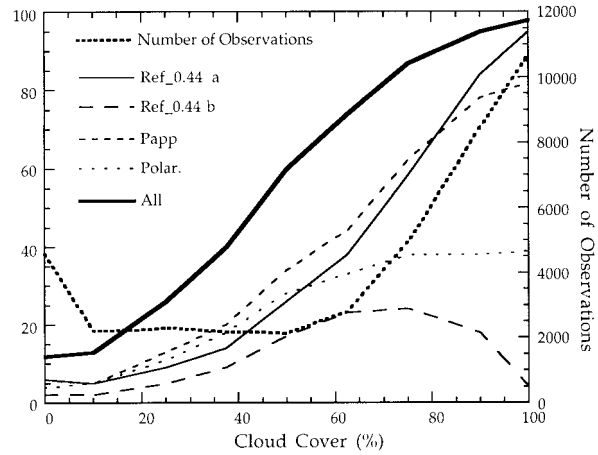

FIG. 9. Global performance of the cloud detection algorithm. The curves indicate, for each class of synoptic cloud cover, the percentage of POLDER observations that have been declared cloudy (left scale). Another line indicates the number of measurements used for each of the nine cloud cover classes.

es (no false cloud detection), and a large percentage for positive cloud covers.

Figure 9 presents the global performance of the method. The results of each of the individual tests are presented together with its combination. Note that the performance of individual tests is the percentage of pixels above the threshold line in Figs. 4, 5, 7, and 8. In the figure (right scale) is also reported the number of coincident observations that have been used for the statistics. We used more than 4000 ''clear'' observations, about 2000 observations for cloud covers between 1 octant and 5 octants, and up to 11 000 for an overcast cloud cover.

According to the figure, the percentage of false alarms is 12% and each test seems to participate roughly equal to this number. The percentage for a 1 octant cloud cover is 13%, which indicates that such cloud covers are hardly ever detected by the method. The percentage increases rapidly and reaches 60% of detection for a 4 octants (50%) cloud cover and 85% for a 6 octants. Each of the four tests participate to these percentages. The blue channel tests are less efficient than the others for the small cloud cover, but more efficient for the large ones. Note that the second of the two blue channel tests is not efficient for large cloud covers, because these situations have a spectrally neutral reflectance. The polarization-based test is rather efficient for small covers but the statistics saturate at about 40% for cloud covers greater than 60%. This is because this test cannot detect ice clouds and because the needed viewing geometry is sampled in only 60% of POLDER acquisitions.

To investigate each test's capabilities further, we make use of the cloud type reports. The cloud observations are classified into three main classes (low, medium, and high) with further cloud-type indication that we did not use here. We only used the surface observations when only one cloud layer was observed. As a consequence, we do not show any statistics for an overcast low or medium cloud layer, since the high cloud cover is then unknown.

Figure 10a shows the cloud detection statistics for the blue channel tests (both tests are combined here). It shows that these tests are much more efficient for low clouds than for high clouds, which is explained by the fact that the optical thickness and therefore the reflectance of high clouds is generally smaller than that of low clouds.

Figure 10b is for the apparent pressure test. When this test was developed, it was anticipated that it would be more efficient for high clouds than for low clouds because the former have a lower pressure (Bréon and Bouffiès 1996). The statistics show that it is not the case. The results are similar for low and high clouds, and slightly better for medium clouds. This must be analyzed together with Fig. 10a results. High clouds seem to have, on average, a larger transmission than low clouds, which reduces their effect on the apparent pressure.

The polarization test results are shown in Fig. 10c. As anticipated, this test does not detect any high cloud because they are made of ice particles. The results for medium and low clouds are similar, which indicates that medium clouds include water droplets in most cases. Again, the saturation of the statistics for large cloud cover is a result of the viewing geometry sampling.

The full cloud detection method is much more efficient for low and medium clouds than for high clouds (Fig. 10d). Overcast high clouds are detected in about 75% of the cases.

6. Discussion

The comparison of satellite estimates of cloud coverage with surface observations raises the question of their different field of view. The POLDER pixel is about 6×6 km^2, which is smaller than the surface observer field of view in most cases. There is some ambiguity, therefore, in the case of small but positive cloud cover. Such surface observation may result from a cloud field of scattered cumulus, or from stratiform clouds over the horizon. In the former case, there are some clouds in the POLDER pixel and we wish a positive cloud detection; in the latter case, the pixel is cloud free. We note, however, that when a cloud is seen by the surface observer, there is some contamination of the incoming solar radiance by side illumination. In such case, the pixel is not reliable for surface or aerosol inversion and should be rejected for further processing. Nevertheless, the differences in field-of-view yield some uncertainty in our validation procedure for the smaller positive cloud coverage (i.e., 1 or 2 octants). On the other hand, there is no such ambiguity for the bins corresponding to ''clear'' or fractional cloud cover larger than 3 oc-

2+54/.240,+4.-7&3623+-.- !"#"! "$!#(')%

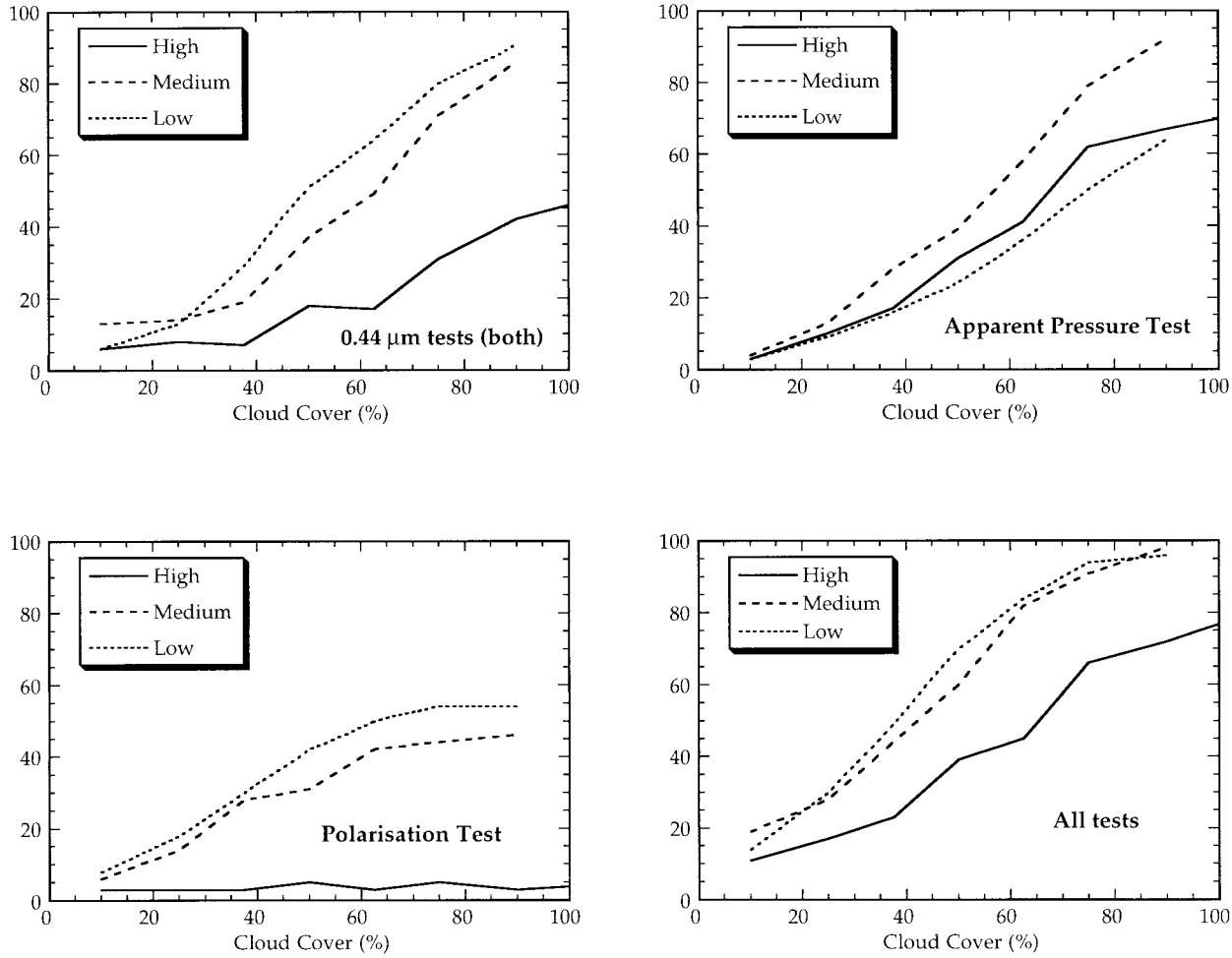

FIG. 10. Same as Fig. 9 but for three classes of clouds (low, medium, and high) as classified by the surface observer. (a) The blue channel tests (combined), (b) the apparent pressure test, (c) the polarization based test, and (d) their combination.

tants. For such cases, the uncertainty in the validation procedure results from the time matching and the faulty cloud reports. This can only worsen the statistics and one can say that the detection algorithm is better (by an unknown amount) than indicated by the statistics. Besides, the validation procedure is an excellent tool to adjust the threshold or to compare the performance of different cloud detection methods because the ''noise'' on the cloud-cover reports is fully uncorrelated with POLDER measurements.

As said above, one known case for which the method will fail is clear, snow-covered pixels when the viewing geometry does not permit the polarization test. In such cases, the pixel will be recognized cloudy by the blue channel test and no reclassification will be made. This was considered as an acceptable burden for the objective of mapping the surface reflectance. Snow-covered pixels are mostly found in high latitude areas, which are frequently observed by polar satellites such as ADEOS. The large number of observation makes it possible to reject some of them when there is a doubt on the cloud or snow presence.

The statistics indicate that the algorithm performances are poor in the case of small cloud coverage. This may be partly due to the imperfect match of field-of-view between the surface and satellite observations. The main cause, however, is most probably the difficulty of recognizing the signature of a cloud when its influence on the satellite measurement is small. We note that, for the further processing of POLDER measurements, this perturbation may be acceptable.

One may argue that the dataset used to define the threshold (section 4) is the same as the one used for the validation (section 5). We believe that the number of satellite–surface matches (more than 20 000) used for the validation is large enough to prevent significative biases. Besides, the statistics presented above have been computed for one month of matches that were not used for the initial selection of the thresholds. The results were very similar. Therefore, we believe that the sta-

2+54/.240,+4.-7&3623+-.- !"#"! "$!#(')%

tistics shown above are representative of the test global skill, although they may be of better or lower accuracy depending on the surface and/or cloud type.

Figure 9 indicates that the probability of cloud detection increases with the cloud cover. The probability of detection is above, but not very different than the 1:1 line. Therefore, one may want to use the algorithm, or a similar one, to evaluate the cloud cover on a statistical basis. However, the curves of Fig. 10 are the result of a combination of observations acquired in very different areas. The statistical results may vary greatly with the area, as a function of the cloud-type occurrence and the surface reflectance properties. Therefore, it is not advisable to use the algorithm to estimate the cloud cover resulting from broken cloudiness.

7. Conclusions

The POLDER instrument provides multispectral, multidirectional, and polarization measurements of the top of the atmosphere reflectances. All measurements are processed to generate estimates of various surface and atmospheric parameters. The first step of the processing is cloud detection. This paper described the cloud detection method, which has been developed for POLDER. The classical methods cannot be applied because the instrument lacks thermal infrared channels. On the other hand, the existence of a blue channel, differential absorption bands, and the polarization capabilities of POLDER allow novel and efficient algorithms for the cloud detection.

The quantitative evaluation of the algorithm performance is evaluated using a large set of coincident POLDER measurements and surface synoptic observations. Despite some uncertainty resulting from the unmatching fields of view, the proposed evaluation method is well suited because 1) it uses a fully independent set of data and 2) it can be applied to large datasets with limited human work.

The ability of the algorithms to recognize a cloud-contaminated pixel increases with the cloud cover (Fig. 9). About 10% of clear pixels are incorrectly declared cloudy, a large fraction of which resulting from surface snow cover. For a given cloud cover, the detection is more efficient for low and medium clouds than for high clouds.

Acknowledgments. The surface observations that are used in this paper have been provided by Meteo-France in the framework of the POLDER program. We thank H. El Mezdari for the management of the database and G. Liberti for useful discussions. The results presented in this paper were obtained using data from CNES's POLDER on board NASDA's ADEOS.

REFERENCES

Bowker, D. E., R. E. Davis, D. L. Myrick, K. Stacy, and W. T. Jones, 1985: Spectral reflectances of natural targets for use in remote sensing studies. NASA Reference Publ. 1139, 181 pp.

Bréon, F. M., and S. Bouffiès, 1996: Land surface pressure estimate from measurements in the oxygen a absorption band. *J. Appl. Meteor.,* **35,** 69–77.

——, and Ph. Goloub, 1998: Cloud droplet effective radius from spaceborne polarization measurements. *Geophys. Res. Lett.,* **25,** 1879–1882.

Buriez, J. C., and Coauthors, 1997: Cloud detection and derivation of cloud properties from POLDER. *Int. J. Remote Sens.,* **18,** 2785–2813.

Derrien, M., B. Farki, L. Harang, H. Le Gléau, A. Noyalet, D. Pochic, and A. Sairouni, 1993: Automatic cloud detection applied to NOAA-11/AVHRR imagery. *Remote Sens. Environ.,* **46,** 246–267.

Deschamps, P. Y., F. M. Bréon, M. Leroy, A. Podaire, A. Bricaud, J. C. Buriez, and G. Seze, 1994: The POLDER mission: Instrument characteristics and scientific objectives. *IEEE Trans. Geosci. Remote Sens.,* **32,** 598–615.

Goloub, Ph., J. L. Deuze, M. Herman, and Y. Fouquart, 1994: Analysis of the POLDER polarization measurement performed over cloud cover. *IEEE Trans. Geosci. Remote Sens.,* **32,** 78–88.

Leroy, M., and Coauthors, 1997: Retrieval of atmospheric properties and surface bidirectional reflectances over the land from POLDER. *J. Geophys. Res.,* **102,** 17 023–17 037.

Saunders, R. W., and K. T. Kriebel, 1988: An improved method for detecting clear sky and cloudy radiances from AVHRR data. *Int. J. Remote Sens.,* **9,** 123–150; Errata, **9,** 1393–1394.

Simpson, J. J., and J. I. Gobat, 1996: Improved cloud detection for daytime AVHRR scenes over land. *Remote Sens. Environ.,* **55,** 21–49.

Visa, A., and J. Iivarinen, 1997: Evolution and evaluation of a trainable cloud classifier. *IEEE Trans. Geosci. Remote Sens.,* **35,** 1307–1315.

2+54/.240,+4.-7&3623+-.- !"#"! "$!#(')%